

Evanescent-wave amplification studied using a bilayer periodic circuit structure and its effective medium model

Ruopeng Liu, Bo Zhao, Xian Qi Lin, Qiang Cheng, and Tie Jun Cui*

Center for Computational Electromagnetics and the State Key Laboratory of Millimeter Waves, Department of Radio Engineering, Southeast University, Nanjing 210096, People's Republic of China

(Received 14 June 2006; revised manuscript received 3 December 2006; published 27 March 2007)

In this paper, we present both theoretical analysis and experimental verification of evanescent-wave amplification by using a bilayer periodic circuit structure and its effective medium model. We propose a series-shunt capacitor (C - C) structure to simulate a magnetic plasma, whose permittivity is positive and permeability is negative, and a series-shunt inductor (L - L) structure to simulate an electric plasma, whose permittivity is negative and permeability is positive, in which the structure cells are not required to be electrically small. In addition, we derive and define an effective permittivity and permeability for the C - C and L - L structures in closed forms, which are completely different from the published ones. When the two structures are cascaded together to form a bilayer structure, we show that evanescent waves which exist in two single layers independently can be amplified exponentially if a certain resonant condition is satisfied. Such a resonant condition is equivalent to the antimatching condition for the permittivity and permeability of the effectively electric and magnetic plasmas. To show the accuracy of this equivalent medium model, we compare both circuit-simulation results for the C - C and L - L structures and theoretical-prediction results for the effective magnetic and electric plasmas, which have excellent agreement. Finally, we design an experiment using lumped capacitors and inductors mounted on a printed circuit board to verify the amplification of evanescent waves sufficiently. The measurement results have good agreement with the simulation results.

DOI: [10.1103/PhysRevB.75.125118](https://doi.org/10.1103/PhysRevB.75.125118)

PACS number(s): 78.20.Ci, 41.20.Jb, 84.40.Az, 42.25.Bs

I. INTRODUCTION

Recently, artificial materials with both negative permittivity and negative permeability in a certain frequency band have attracted great interest in both scientific and industrial communities. Such materials are termed as left-handed materials (LHM),¹ which have not received much attention due to their absence in nature until recently, when the negative refraction has been demonstrated experimentally by using periodic structures containing metallic rods and split-ring resonators (SRRs).² Inspired by the experimental results, numerous researches have been devoted to understanding the physical essences of LHM. One of the most important properties of LHM is the ability to restore the amplitude of evanescent waves, which leads to a super-resolution imaging³ through surface plasmon between right-handed material (RHM) and LHM slab. It was shown by Pendry that all evanescent components emitted from a source can be focused and restored in amplitude by a flat LHM slab to make a perfect lens when the relative permittivity and permeability are both strictly equal to -1 .³ However, this condition will never be reached in practice.⁴ The reconstruction of evanescent waves can be observed only when the LHM lens has a very small loss and retardation with respect to the RHM background.^{5,6} Because of these theoretical analysis and predictions, a clear experimental verification of the evanescent-wave amplification (EWA) becomes very important and desirable.

Recently, several experimental studies on EWA have been reported. In Ref. 7, growing evanescent waves are observed in a cutoff rectangular waveguide, which is loaded with an inductive iris and a capacitive post. Later, the evanescent-wave enhancement has been studied by inserting a structured

SRR metamaterial inside a rectangular waveguide.⁸ However, the EWA phenomenon observed in these experiments is quite weak due to the relatively large loss in the SRR metamaterial.

Another approach to implement LHM is to use a periodic structure which comprises inductor- and capacitor-loaded transmission lines.⁹ It has been shown that such structured LHM have much smaller loss and have been applied in some new microwave components and antennas.¹⁰ Simulation and experimental studies have been conducted on the enhancement of evanescent waves using the planar metamaterials.¹¹⁻¹³ In such experiments, a point voltage source drives a circuit network on a printed circuit board (PCB) which simulates a LHM slab embedded in RHM. Strong surface waves are observed on the RHM-LHM interfaces in both simulation and experimental results,¹¹⁻¹³ which can verify the amplification of evanescent waves in a certain extent.

In the above experiments, however, both the propagating waves and evanescent waves are emitted by the voltage source and they are interlaced together. Hence, it is not sufficiently evident to verify the EWA phenomenon. In order to restore pure evanescent waves using the planar metamaterials, another experiment has been proposed with the aid of a planar waveguide,¹⁴ in which a significant enhancement in amplitude of evanescent waves was demonstrated. Here again, due to the strongly local resonance, the exponential increase and decay of internal fields were not observed in such an experiment.

In addition to the LHM-RHM approach for EWA, Alú and Engheta proposed another way to restore evanescent waves using bilayered epsilon-negative (ENG) and mu-negative (MNG) materials theoretically.¹⁵ In this study, ideal homoge-

neous ENG and MNG materials were used and a transmission-line model was introduced to analyze the homogeneous ENG-MNG bilayer.¹⁵ It is shown theoretically that the bilayer could produce a tunneling effect through EWA.¹⁵ Based on such a theoretical study, an experimental demonstration of the transparency in ENG-MNG bilayer has further been presented using composite right- and/or left-handed (CRLH) transmission lines.¹⁶ However, the amplification of evanescent waves was obviously still not observed.

Besides the experiments in microwave regime, a super-resolution imaging experiment was implemented at the optical regime by using a slim silver slab,¹⁷ in which the sub-wavelength imaging is realized due to the surface plasmon of silver in the near-field region.

In this paper, we propose a direct way to study the EWA phenomenon using a bilayer periodic circuit structure and its effective medium model. We present a series-shunt capacitor (*C-C*) structure to simulate a magnetic plasma and a series-shunt inductor (*L-L*) structure to simulate an electric plasma. Therefore, waves in either single *C-C* or *L-L* structure will decay exponentially; namely, only evanescent waves are supported in such single *C-C* or *L-L* structures. However, when a junction between the *C-C* and *L-L* structures is made, an antimatching of effective permittivity and permeability at the junction can be achieved through careful calculation according to the equivalent medium model, which will lead to a resonance. More specifically, the energy will “tunnel” through the junction because of this kind of resonance. If there is no strong reflection at the terminal load, a plasmon-like behavior of fields will appear around the junction, where an exponentially increasing-decreasing field distribution is observed. We have also derived the effective permittivity and permeability of the *C-C* and *L-L* structures in closed forms. The theoretical prediction results of the effective magnetic and electric plasmas have excellent agreement to the circuit simulation results of real structures. Finally, we propose an experiment using lumped capacitors and inductors mounted on PCB to verify the EWA phenomenon.

II. STRUCTURED MAGNETIC AND ELECTRIC PLASMAS

A. *C-C* and *L-L* structures

We use one-dimensional periodic *LC*-network structures to simulate an artificial media. Figure 1 shows the *C-C* and *L-L* structures, where n represents the number of cells in each structure. We specify $n=8$ in the following discussions as an example. In terms of indicated structures, *C-C* represents a magnetic plasma and *L-L* is equivalent to an electric plasma.

B. Evanescent-wave behaviors

Since the *C-C* and *L-L* structures simulate magnetic and electric plasmas, respectively, the two structures will not allow wave propagation in the whole frequency band. Only evanescent waves exist in those two structures. Figure 2 shows the transmission coefficients of the independent *C-C* and *L-L* structures simulated using Agilent’s advanced

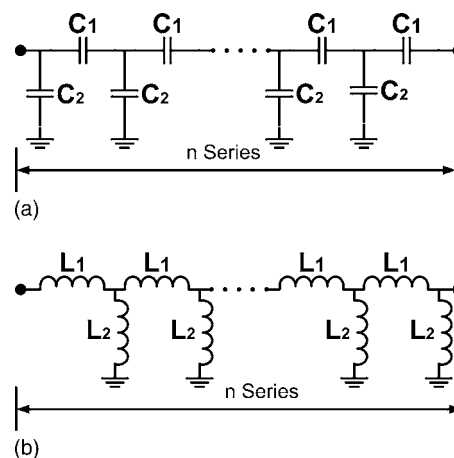


FIG. 1. The *C-C* and *L-L* structures. (a) The *C-C* structure. (b) The *L-L* structure.

design system (ADS) to validate our remarks, where $C_1=C_2=10$ pF and $L_1=L_2=10$ nH.

Since no propagating waves exist in these two structures, the S_{21} parameters are all under -60 dB and only evanescent waves are supported. To further verify the evanescent behavior, we choose a frequency at 502.3 MHz and compute the voltage values at each unit junction in the structure using ADS. The voltage distribution along the *C-C* or *L-L* structure is shown in Fig. 3(a) with an absolute scale and in Fig. 3(b) with a logarithm scale, which clearly verifies the exponentially decayed distribution.

C. Equivalent magnetic and electric plasmas

To link the periodic circuit structures with homogeneous media, we set up an effective medium model by defining equivalent permittivity and permeability of the *C-C* and *L-L* structures.

Consider an infinite periodic *C-C* or *L-L* structure. The effective permittivity and permeability of such a structure can be easily obtained from the wave vector k and the wave impedance Z . For the *C-C* structure, we derive the wave vector k from Fig. 2(a) using the *LC*-network theory as

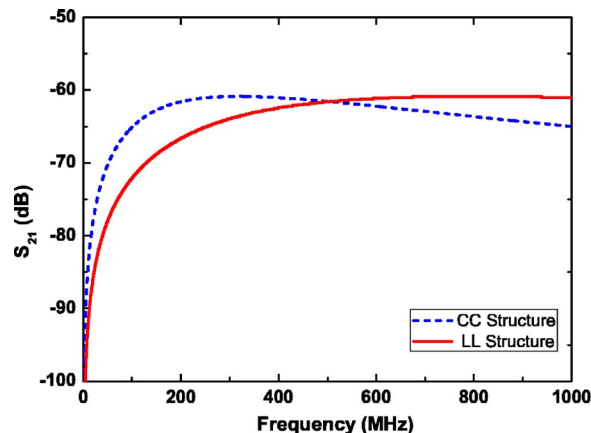
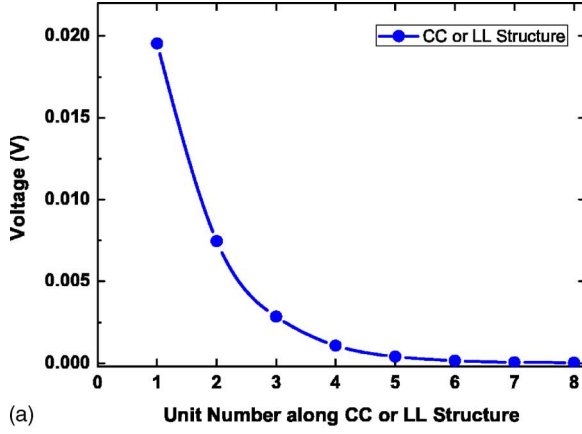
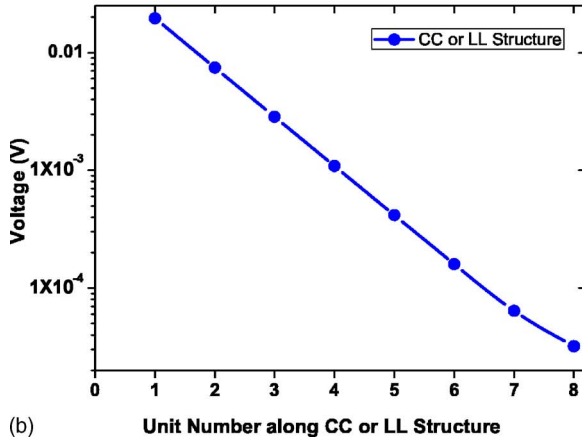


FIG. 2. (Color online) The transmission coefficients of the *C-C* and *L-L* structures in the frequency band from 0 to 1 GHz.



(a)



(b)

FIG. 3. (Color online) The voltage distributions along the C - C and L - L structures. (a) In absolute scale for voltage. (b) In logarithmic scale for voltage.

$$k = \omega \sqrt{\epsilon \mu} = i \theta_C / p, \quad (1)$$

where

$$\theta_C = 2 \ln(\sqrt{C_2/4C_1} + \sqrt{C_2/4C_1 + 1}), \quad (2)$$

and p is the length of unit cell. Based on the wave vector, it is very easy to derive the wave impedance as

$$Z = \sqrt{\mu/\epsilon} = i[\exp(\theta_C) - 1]/(\omega C_2). \quad (3)$$

Therefore, we can extract the effective permittivity and permeability of the C - C structure from Eqs. (1) and (3),

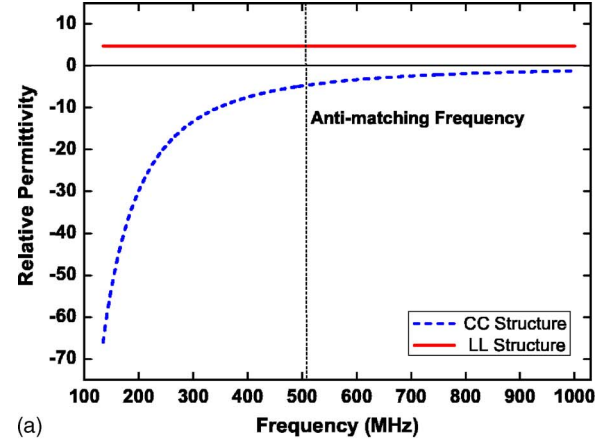
$$\epsilon_{CC} = C_2 \theta_C / \{\exp(\theta_C) - 1\} p, \quad (4)$$

$$\mu_{CC} = -\theta_C [\exp(\theta_C) - 1] / (\omega^2 C_2 p). \quad (5)$$

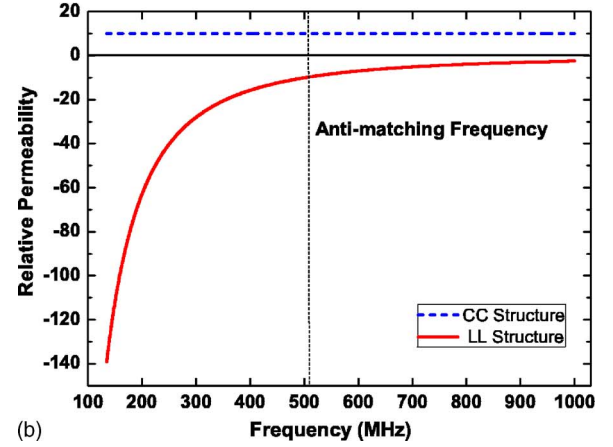
From Eqs. (4) and (5), we can see that the permittivity is always positive while the permeability is always negative. In other words, the C - C structure is a kind of magnetic plasma.

Similarly, for the L - L structure, we derive the effective permittivity and permeability as

$$\epsilon_{LL} = -\theta_L [\exp(\theta_L) - 1] / (\omega^2 L_1 p), \quad (6)$$



(a)



(b)

FIG. 4. (Color online) The equivalent permittivity and permeability of the C - C and L - L structures. (a) Permittivity. (b) Permeability.

$$\mu_{LL} = L_1 \theta_L / \{\exp(\theta_L) - 1\} p, \quad (7)$$

where

$$\theta_L = 2 \ln(\sqrt{L_1/4L_2} + \sqrt{L_1/4L_2 + 1}), \quad (8)$$

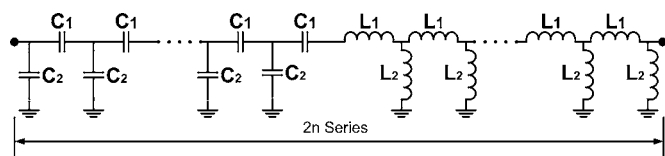
and p is the length of unit cell. From Eqs. (6) and (7), we can clearly find that the L - L structure is a kind of electric plasma.

Figure 4 demonstrates the equivalent permittivity and permeability for the C - C and L - L structures, respectively, which will be very important in the following medium-model discussions in Sec. IV.

III. EWA PHENOMENON IN C - C AND L - L BILAYER PERIODIC STRUCTURE

Since we have extracted an equivalent medium model of the C - C and L - L structures, the EWA phenomenon is expected by putting them together to form a bilayer periodic structure, as illustrated in Fig. 5.

For the CC - LL bilayer structure, we perform an ADS circuit simulation to calculate the transmission coefficient. We choose $C_1 = C_2 = 10$ pF and $L_1 = L_2 = 10$ nH in our simulation. Figure 6 shows the simulation results of transmission coefficients for the two cases of $n=4$ and $n=8$.


 FIG. 5. A *CC-LL* bilayer structure.

From Fig. 6, there is an obvious peak at the frequency of 502.3 MHz. The transmission coefficient in both 8 and 16 unit cases is nearly 0 dB which means a total transmission. This frequency, however, is clearly located at the cutoff frequency area (below -60 dB) when compared with the simulation results for single *C-C* and *L-L* structures in Fig. 2. Consequently, we remark that the evanescent wave does transmit through this structure according to the results presented above.

To further confirm the EWA phenomenon in the bilayer periodic structure, we also simulate the voltage distribution along the bilayer structure using ADS, which is shown in Figs. 8(b) and 8(c). Comparing Fig. 8 with Fig. 3, it is evident that the amplitude of evanescent waves increased exponentially in the first layer of the bilayer periodic structure and then decreased exponentially in the second layer. Such a distribution is due to a strong surface plasma resonance between the interface of *C-C* and *L-L* structures, and the resonant frequency is actually determined by the series and shunt resonances,

$$\omega_0 = 1/\sqrt{L_1 C_1} = 1/\sqrt{L_2 C_2}. \quad (9)$$

Hence, we observe the surface plasmon under the microwave regime in the periodic circuit structure. This is analogous to what happened to an evanescent wave in optical regime in RHM when it impinges on a silver half-space which will also peak at resonance.

The physical insight of the total transmission (or the EWA phenomenon) in the bilayered circuits can be explained as follows. At the resonant frequency, the four capacitors and/or inductors C_1 , C_2 , L_1 , and L_2 at the interface become resonant, and hence they are actually inactive in the whole circuit. As

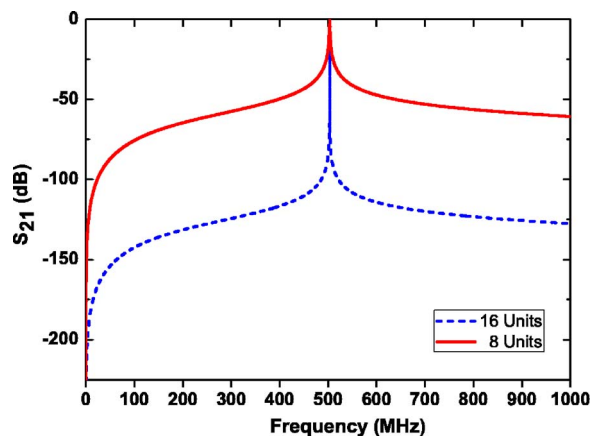


FIG. 6. (Color online) The transmission coefficients of the *CC-LL* bilayer structures, where the EWA phenomenon is observed at the cutoff frequency for both *C-C* and *L-L* structures.

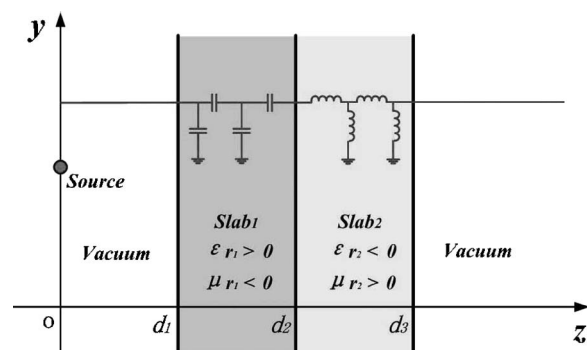


FIG. 7. A source located before a magnetic-electric plasma bilayer structure.

a consequence, the other four capacitors and/or inductors C_1 , C_2 , L_1 , and L_2 close to the interface become resonant again, and so on. Finally, all capacitors and inductors in the whole circuits are inactive, and hence the input signal can be totally transmitted in this manner. We emphasize that this resonance can happen only when the two independent *C-C* and *L-L* structures are connected together; namely, the resonance can be achieved only between the two independent structures but not inside any single structure separately. This explains why the voltage distribution is increasing-decreasing exponentially, which also reveals to us the essence of surface plasmon.

When the number of series increases from 8 ($n=4$) to 16 ($n=8$), the peak (resonant) frequency remains the same based on the above discussion, as shown in Fig. 6. Thus, the resonant frequency is independent of the number of cells, i.e., the length of structure. This is also a well-known property for the plasma resonance. However, the variation of structure length (or cell number n) will affect the bandwidth of the peak. From Fig. 6, the longer the structure is, the narrower the bandwidth is, and the higher the quality (Q) factor is.

IV. THEORETICAL STUDY OF EWA IN BILAYER SLAB

According to the above discussions, the *C-C* and *L-L* structures are equivalent to magnetic and electric plasmas. Hence, the *CC-LL* bilayer structures shown in Fig. 5 can be regarded as bilayer slabs residing in free space, as shown in Fig. 7. Here, the first slab with the relative permittivity ϵ_{r1} and relative permeability μ_{r1} denotes the *C-C* magnetic plasma, the second slab with the relative permittivity ϵ_{r2} and relative permeability μ_{r2} represents the *L-L* electric plasma, and the free space indicates the matching-impedance terminals of the *CC-LL* bilayer structure.

As shown in Fig. 7, the whole space is divided into four regions: 0, 1, 2, and 3. We assume a TE-polarized plane wave as the incident wave from free space (region 0) to the bilayer slabs, and the electric fields in all regions have only y components under the Cartesian coordinate shown. We write the incident electric field as

$$E^{inc} = E_0 e^{ik_y y} e^{ik_0 z}. \quad (10)$$

Then, the plane-wave reflection and transmission coefficients of the layered slabs can be derived as¹⁸

$$R = (a + b)e^{i2k_{0z}d_1}/(d + e), \quad (11)$$

$$T = c/(d + e), \quad (12)$$

where

$$a = r_{01} + r_{01}r_{12}r_{13}e^{i2\phi_2},$$

$$b = r_{12}e^{i2\phi_1} + r_{23}e^{i2(\phi_1+\phi_2)},$$

$$c = t_{01}t_{12}t_{23}e^{i(\phi_1+\phi_2)}e^{i(k_{0z}d_1-k_{3z}d_3)},$$

$$d = 1 + r_{12}r_{23}e^{i2\phi_2},$$

$$e = r_{01}r_{12}e^{i2\phi_1} + r_{01}r_{23}e^{i2(\phi_1+\phi_2)},$$

and $k_{mz} = \sqrt{k_m^2 - k_y^2}$ is the longitudinal wave number in region m ; r_{mn} and t_{mn} are Fresnel reflection and transmission coefficients, respectively, with

$$r_{mn} = (\mu_n k_{mz} - \mu_m k_{nz}) / (\mu_n k_{mz} + \mu_m k_{nz}),$$

$$t_{mn} = (2\mu_n k_{mz}) / (\mu_n k_{mz} + \mu_m k_{nz}),$$

in which $m, n = 1, 2, 3$, $\phi_1 = k_{1z}h_1$, and $\phi_2 = k_{2z}h_2$. Here, $h_1 = d_2 - d_1$ and $h_2 = d_3 - d_2$ represent the thicknesses of two slabs.

When the two slabs have equal thickness ($h_1 = h_2$) and satisfy the following antimatching conditions:

$$\epsilon_{r1} = -\epsilon_{r2} > 0, \quad \mu_{r1} = -\mu_{r2} < 0, \quad (13)$$

we can easily show that the reflection coefficient R is always equal to zero for both propagating waves (k_{0z} is real) and evanescent waves (k_{0z} is imaginary). Under this condition, the bilayer slab is transparent to any incident waves, corresponding to the complete wave tunneling effect.¹⁵

It will be interesting to investigate the physical origins of the tunneling effect. As we know, whether it is propagating or evanescent, the incident wave turns into an evanescent wave when entering the plasma layers. This implies that no propagating waves can be supported by either single slab. The internal electric fields in the two layers are given by

$$E_i = E_0(E_i^+ e^{ik_{iz}z} + E_i^- e^{-ik_{iz}z})e^{ik_y y}, \quad (14)$$

where $i = 1, 2$, and E_i^+ and E_i^- are the forward and backward propagation coefficients in region i . After simple manipulation, we obtain such coefficients as

$$E_1^\pm = \frac{1}{2}(1 \pm p_{10})e^{ik_{0z}d_1}e^{\pm\alpha d_1}, \quad (15)$$

$$E_2^\pm = \frac{1}{2}(1 \mp p_{10})e^{ik_{0z}d_1}e^{\mp\alpha(d_1-2d_2)}, \quad (16)$$

in which $\alpha = \text{Im}(k_{1z}) = \text{Im}(k_{2z})$ and $p_{01} = i\alpha / (\mu_{r1}k_{0z})$. It is clear that the evanescent waves grow exponentially as $e^{\alpha(z-d_1)}$ in region 1 and decay exponentially as $e^{-\alpha(z+d_1-2d_2)}$ in region 2 when transmitting through the slabs. Hence, there exists a peak field value at the interface of the two plasma layers, which is, in fact, the surface plasmon excited by the interac-

tion of source and slabs. It is the surface plasmon that helps to enhance the evanescent waves within the layers and to tunnel the incident waves through the slab region.

We can easily obtain the transmission coefficient through the antimatching bilayer slabs for propagating waves where k_{0z} is real,

$$T = e^{-ik_{0z}(h_1+h_2)}, \quad (17)$$

and that for evanescent waves where k_{0z} is imaginary,

$$T = e^{\text{Im}(k_{0z})(h_1+h_2)}. \quad (18)$$

It is evident that if a source is located at the left boundary of the slabs, the propagating components emitted from the source experience phase compensation, while the evanescent components have their amplitude to be recovered within the two layers. As a result, both components at the exit surface of the slab are exactly the same as they enter the two layers.

From the above theoretical analysis, the physics feature of EWA has very good agreement with the study we have conducted in the bilayer periodic structure earlier. To further justify the theory study and equivalent circuit-medium model, we substitute the equivalent permittivity and permeability in Eqs. (4)–(7) into Eq. (12) to calculate the transmission coefficient and the field distribution along the *CC-LL* bilayer periodic structure again. Figure 8 shows the comparison results of circuit simulation and theoretical prediction, which obviously have excellent agreement so, it is further evidence for EWA observed in a bilayer periodic structure and a validation of the equivalent-medium model.

To understand more profoundly, we investigate the equivalent permittivity and permeability of the *C-C* and *L-L* periodic structures. From Fig. 4, it is obvious that the antimatching resonant condition indicated by Eq. (13) is satisfied for both ϵ and μ at the frequency of 502.3 MHz. This is why a peak occurs at such a frequency in the transmission coefficient, which makes the perfect tunneling.

To study the resonant condition, we substitute Eqs. (4)–(7) into condition (13) which is derived by the field analysis, yielding

$$\epsilon_{CC} = -\epsilon_{LL}, \quad \mu_{CC} = -\mu_{LL}, \quad (19)$$

which are the electric plasma condition and magnetic plasma condition, respectively. Both conditions should be satisfied to make the plasma resonance. After simple derivation, we obtain the electric and magnetic plasma resonant frequencies as

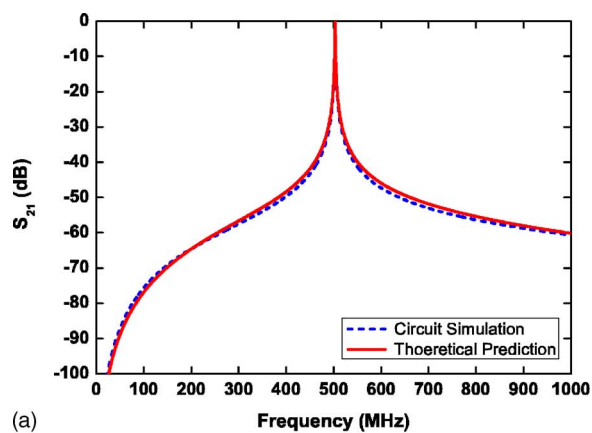
$$\omega_\epsilon^2 = \frac{\theta_L[\exp(\theta_C) - 1]}{\theta_C[\exp(\theta_L) - 1]C_2L_2}, \quad (20)$$

$$\omega_\mu^2 = \frac{\theta_C[\exp(\theta_C) - 1]}{\theta_L[\exp(\theta_L) - 1]C_2L_2}. \quad (21)$$

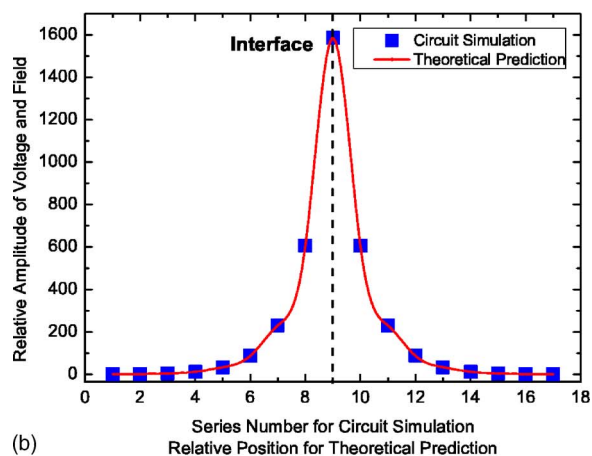
To get the plasma resonance, the electric and magnetic plasma resonant frequencies should be equal. Hence, deriving from $\omega_\epsilon = \omega_\mu$, we obtain the final resonant condition for the *CC-LL* bilayer structure as

$$L_1C_1 = L_2C_2, \quad (22)$$

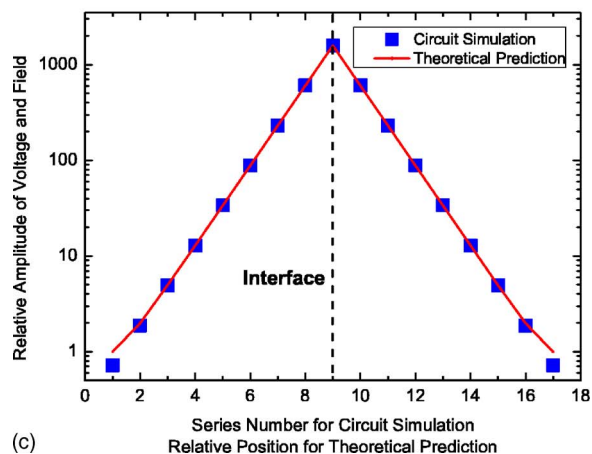
and the corresponding resonant frequency is



(a)



(b)

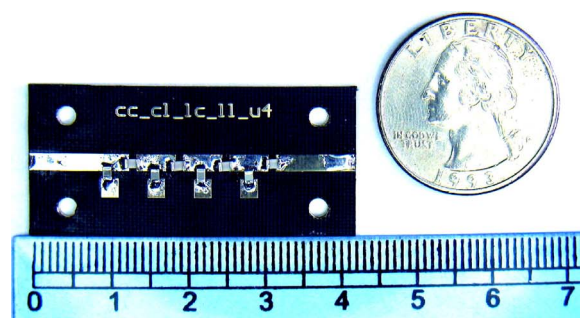


(c)

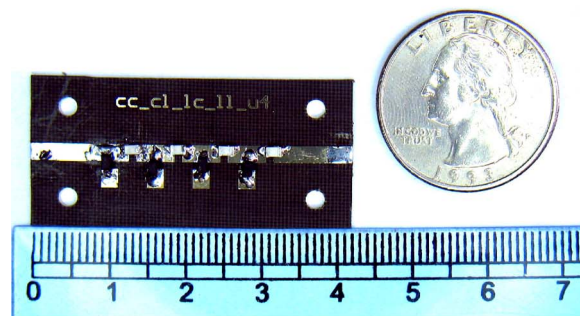
FIG. 8. (Color online) Comparison of theoretical-prediction results with circuit simulation results. (a) The transmission coefficient. (b) The field distribution in absolute scale. (c) The field distribution in logarithm scale.

$$\omega = 1/\sqrt{L_1 C_1} = 1/\sqrt{L_2 C_2}, \quad (23)$$

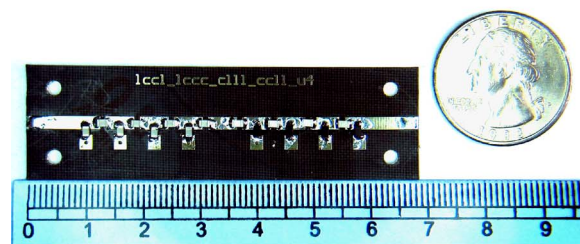
which is exactly the same as the circuit resonant frequency shown in Eq. (9). Therefore, the EWA phenomenon in the periodic circuit system is completely equivalent to that in the theoretical bilayer slabs. Looking into the bilayer structure shown in Fig. 5 again, we find that the EWA nature is the



(a)



(b)



(c)

FIG. 9. (Color online) Pictures of the *C-C*, *L-L*, and *CC-LL* bilayer structures ($n=4$). (a) The *C-C* structure. (b) The *L-L* structure. (c) The *CC-LL* bilayer structure.

resonance of the series and shunt capacitors and inductors, which actually represents the electric plasma resonance and magnetic plasma resonance at the interface.

V. EXPERIMENTAL VERIFICATION OF EWA

To verify the above analysis on EWA both in bilayer periodic circuit structure and in bilayer slabs, we set up a simple experiment using lumped capacitors and inductors connected together. Here, we choose four units for both *C-C* and *L-L* structures and design the value of series capacitor $C_1=8.2$ pF and shunt capacitor $C_2=4$ pF. Similarly, we choose $L_1=10$ nH and $L_2=15$ nH in order to meet the resonant condition at the frequency near 500 MHz. We remark that the parasitical effect of microstrip line on PCB has been considered in the above design.

We mount all components on a PCB board along a microstrip line, as illustrated in Fig. 9. The microstrip line has a width of 2.2 mm, and the length between two lumped components is chosen to be 5 mm. An F4B-1/2 substrate is used, which is made of polytetra-fluoroethylene and glass fiber

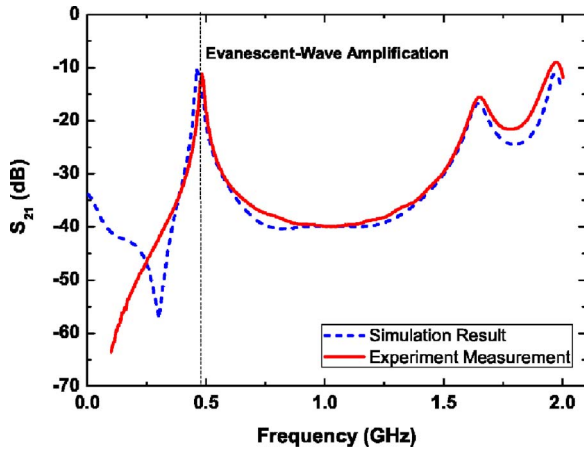
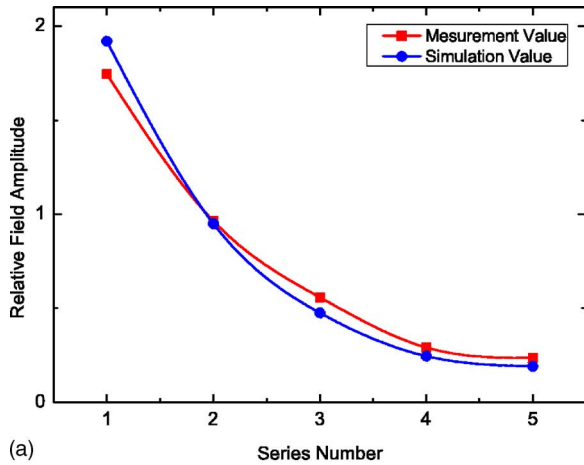
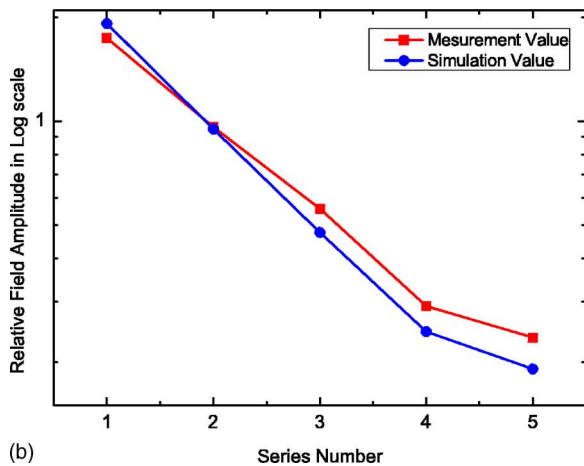


FIG. 10. (Color online) Comparison of the transmission coefficients (S_{21}) between experiment and simulation results.

with the thickness of $h=0.8$ mm and the relative permittivity of $\epsilon_r=2.65$. The microstrip feed lines at two ports with a length of 8 mm and a width of 2.2 mm are selected. The values match 50Ω .

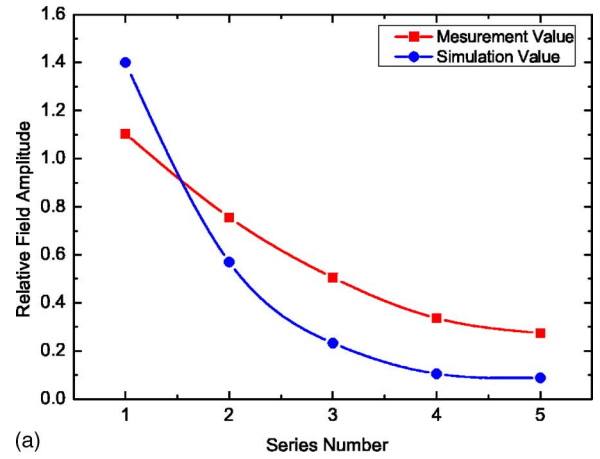


(a)

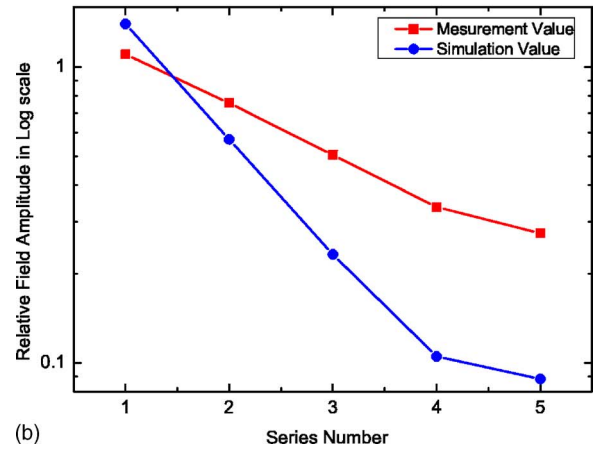


(b)

FIG. 11. (Color online) Experiment and simulation results of the field distributions along the $C-C$ structure. (a) In absolute scale for the electric field. (b) In logarithm scale for the electric field.



(a)



(b)

FIG. 12. (Color online) Experiment and simulation results of the field distributions along the $L-L$ structure. (a) In absolute scale for the electric field. (b) In logarithm scale for the electric field.

We then use an Agilent E5071B vector network analyzer to measure the reflection and transmission coefficients of the $C-C$, $L-L$, and $CC-LL$ bilayer structures, respectively. The measurement result of the scattering parameter S_{21} for the bilayer structure is illustrated in Fig. 10, in which the full-wave simulation result considering the substrate effect using the CST MICROWAVE STUDIO 5.0 is also given for comparison.

From Fig. 10, we observe an obvious peak near the frequency of 500 MHz, which is a cutoff frequency for both $C-C$ and $L-L$ structures. The full-wave simulation and measurement results have good agreement. Thus, it is the evidence to verify the EWA phenomenon experimentally in the circuit model. We remark that the transmission peak in Fig. 10 has been reduced to -10 dB from 0 dB in Fig. 6. This is because the simulation results in Fig. 6 are obtained from the ideally lumped capacitors and inductors using ADS. In real experiment, however, the lumped capacitors and inductors have to be mounted in PCB. Hence, the loss in PCB substrate, the distributed capacitor and inductor of PCB, and the insertion loss caused by SMA in measurement make the drastic reduction of transmission peak.

We further use an electromagnetic probe to measure the electric-field distributions along the $C-C$, $L-L$, and $CC-LL$ bilayer structures, respectively, and compare them with the

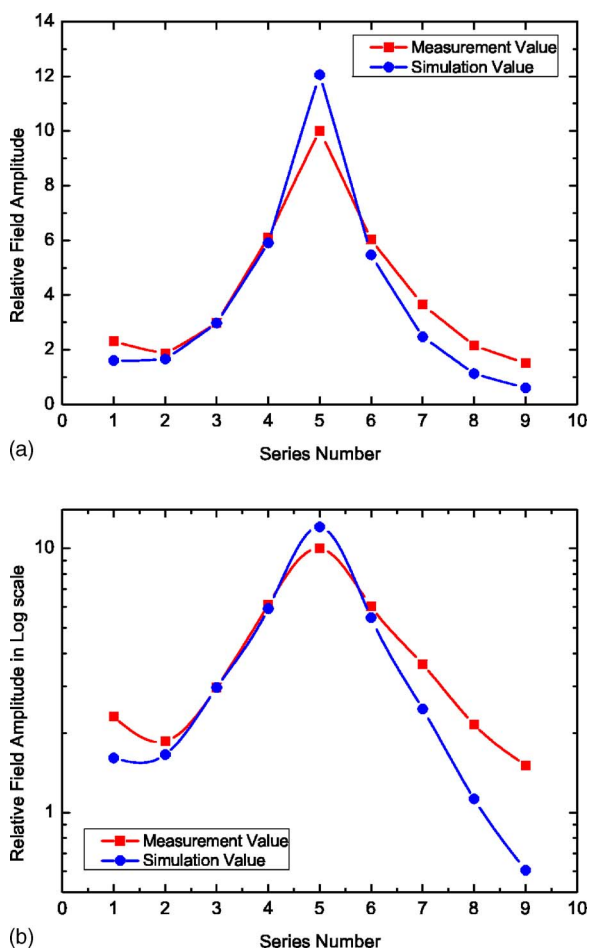


FIG. 13. (Color online) Experiment and simulation results of the field distributions along the *CC-LL* bilayer structure. (a) In absolute scale for the electric field. (b) In logarithm scale for the electric field.

CST simulation results, as illustrated in Figs. 11–13. Here, a short vertical probe is used to detect the vertical electric fields of 1.0 mm above the microstrip line, which is connected to port 2 of the network analyzer. Port 1 is connected to one port of the *C-C*, *L-L*, and *CC-LL* bilayer structures to serve as the excitation. The other port of circuits is matched with the $50\ \Omega$ load.

From Figs. 11 and 12, it is clear that the field amplitudes decay exponentially along both the *C-C* and *L-L* structures. Since small-value inductors are difficult to be achieved exactly, the simulation and measurement results of the *L-L* structure do not meet well, but they are the same in the exponential decay of amplitudes. The experimental results support the conclusion that evanescent waves are generated in the *C-C* and *L-L* structures.

Finally, we demonstrate the electric-field distributions along the *CC-LL* bilayer structure, as shown in Fig. 13. A strong surface wave is observed at the interface between the *C-C* and *L-L* structures. The evanescent waves proved by experiments in Figs. 11 and 12 are amplified exponentially by the fierce resonance generated in both series and shunt components. Considering the earlier analysis and equivalence between the circuit network and medium model, this experiment confirms the EWA phenomenon.

VI. CONCLUSIONS

In this paper, we discuss the EWA phenomenon in bilayer structure composed of *C-C* magnetic plasma and *L-L* electric plasma. We observe EWA and surface plasmon directly from experiments by measuring field and/or voltage distributions and transmission coefficients in the periodic circuit structure. We also derive the resonant condition from the periodic-circuit viewpoint and equivalent bilayer-slab theory, which gives profound understanding of EWA from a structure in nature.

Moreover, EWA may also be important in circuit systems. The evanescent signals can be restored by the plasma resonant to form new “propagation” modes with properties such as high Q factors and energy localizations. Hence, the mechanism proposed in this paper will provide a basic ground to restore evanescent signals in circuits for future work.

ACKNOWLEDGMENTS

This work was supported in part by the National Basic Research Program (973) of China under Grant No. 2004CB719802, in part by the National Science Foundation of China under Grant Nos. 60671015, 60496317, 60225001, and 60621002, and in part by the National Doctoral Foundation of China under Grant No. 20040286010.

*Email address: tjcui@seu.edu.cn

¹V. G. Veselago, *Sov. Phys. Usp.* **10**, 509 (1968).

²R. A. Shelby, D. R. Smith, and S. Schultz, *Science* **292**, 77 (2001).

³J. B. Pendry, *Phys. Rev. Lett.* **85**, 3966 (2000).

⁴N. Garcia and M. Nieto-Vesperinas, *Phys. Rev. Lett.* **88**, 207403 (2002).

⁵S. A. Ramakrishna and J. B. Pendry, *J. Mod. Opt.* **49**, 1747 (2002).

⁶T. J. Cui, Q. Cheng, W. B. Lu, Q. Jiang, and J. A. Kong, *Phys. Rev. B* **71**, 045114 (2005).

⁷M. Stickel and G. V. Eleftheriades, *J. Appl. Phys.* **97**, 124910

(2005).

⁸B. I. Popa and S. A. Cummer, *Phys. Rev. E* **73**, 016617 (2006).

⁹A. Grbic and G. V. Eleftheriades, *IEEE Trans. Antennas Propag.* **51**, 2604 (2003).

¹⁰C. Caloz and T. Itoh, *Electromagnetic Metamaterials: Transmission Line Theory and Microwave Applications* (Wiley, New York, 2004).

¹¹A. Grbic and G. V. Eleftheriades, *Appl. Phys. Lett.* **82**, 1815 (2003).

¹²A. Grbic and G. V. Eleftheriades, *Phys. Rev. Lett.* **92**, 117403 (2004).

¹³T. J. Cui, Q. Cheng, Z. Z. Huang, and Y. Feng, *Phys. Rev. B* **72**,

- 035112 (2005).
- ¹⁴T. J. Cui, X. Q. Lin, Q. Cheng, H. F. Ma, and X. M. Yang, Phys. Rev. B **73**, 245119 (2006).
- ¹⁵A. Alú and N. Engheta, IEEE Trans. Antennas Propag. **51**, 2558 (2003).
- ¹⁶T. Fujishige, C. Caloz, and T. Itoh, Microwave Opt. Technol. Lett. **46**, 476 (2005).
- ¹⁷N. Fang, H. Lee, C. Sun, and X. Zhang, Science **308**, 534 (2005).
- ¹⁸W. C. Chew, *Waves and Fields in Inhomogeneous Media* (Van Nostrand Reinhold, New York, 1990).